α-^{16}O and α-^{15}N optical potentials in the range between 0 and 150 MeV

H. Abele and G. Staudt
Physikalisches Institut der Universität Tübingen, D 7400 Tübingen, Germany
(Received 14 April 1992)

A unified description of scattering cross sections as well as bound and quasibound states for the systems $\alpha + {}^{16}$O and $\alpha + {}^{15}$N is presented. Optical potentials have been extracted from the analysis of elastic α-scattering data on ^{16}O and ^{15}N in a wide range of energies. Special emphasis was given to the $\alpha + {}^{16}$O scattering at energies near the Coulomb barrier. The real part of the potential was calculated using the double-folding procedure. Effective nucleon-nucleon interactions with different density dependence as well as zero-range and finite-range knock-on-exchange potentials are investigated. The dispersive part of the real potential was calculated using the dispersion relation of the optical potential. Together with the dominating channel potential it reproduces the observed energy dependence of the volume integral of the real part of the potential. We calculate the energies and other properties of bound and resonance α-cluster states in ^{20}Ne and ^{19}F and find good agreement with the experimental data. As an application of the derived energy dependence of the optical potential we calculate $\alpha + {}^{16}$O excitation functions in the energy range from 10 to 30 MeV. In this region strong resonances in the compound system are observed.

PACS number(s): 24.10.Ht, 25.55.Ci

I. INTRODUCTION

During the past several decades the nuclear systems $\alpha + {}^{16}$O and $\alpha + {}^{15}$N have been studied intensively, both experimentally and theoretically. Up to an alpha energy of about 20 MeV a large amount of elastic-scattering data have been collected [1–9]. The main purpose of these experiments was to extract resonance energies, widths, and spins of states of the compound nuclei ^{20}Ne and ^{19}F. In the range between about 20 and 30 MeV, data have been taken by several authors [10–13]. In this range an anomalously large angle scattering (ALAS) is observed for many target nuclei including ^{16}O and ^{15}N. The interpretation of the ALAS effect and the rainbow scattering at higher energies has played a decisive role in establishing a unique α-nucleus optical potential [14]. For the $\alpha + {}^{16}$O system such an optical potential was constructed by Michel *et al.* [15]. This potential, which has only two smoothly varying energy-dependent parameters, describes successfully the $\alpha + {}^{16}$O elastic scattering data in the energy range between about 30 and 150 MeV.

Differential cross sections for the elastic scattering of α particles on ^{15}N and ^{16}O have been measured by Abele *et al.* [16] at $E_\alpha = 48.7$ and 54.1 MeV. The experimental results were analyzed in terms of the optical model using the double-folding approach [17] for the real part of the potential. This potential in connection with an imaginary part expressed in terms of Fourier-Bessel functions gives a precise description of the data. The folding potential is close to the real part of the empirical potential of Michel *et al.* [15] for both its shape and energy dependence.

First, Sünkel and Wildermuth [18] calculated differential cross sections of $\alpha + {}^{16}$O elastic scattering at about 20 MeV taking into account the overall antisymmetrization within the resonating-group method (RGM). Ohkubo *et al.* [19] studied the $\alpha + {}^{16}$O scattering at $E_\alpha \approx$ 20–25 MeV from the viewpoint of the alpha-cluster structure adopting the orthogonality-condition model (OCM). Leeb and Schmid [20] tested the fishbone optical model which is related to RGM on $\alpha + {}^{16}$O scattering. Extensive RGM calculations were carried out by Wada and Horiuchi [21]. They aimed to describe the $\alpha + {}^{16}$O elastic scattering and the $\alpha \otimes {}^{16}$O cluster states in ^{20}Ne in a unified way. The results of the calculations are in good agreement with the experimental cross section data over a wide range of energies. The equivalent local potential derived from RGM is found to be very similar to the optical potential of Michel *et al.* [15] which, as mentioned above, agrees with the double-folding potential used by Abele *et al.* [16]. Recently, the complex internucleus potential for the $\alpha + {}^{16}$O system was investigated by Yamaguchi in the framework of the totally antisymmetrized many-body theory [22]. Both real and imaginary parts of the theoretical potential coincide well with the phenomenological optical potential which is determined by the experimental results.

At low incident α energies a strong energy dependence of the real part of the α-nucleus interaction is expected [23]. RGM [24] as well as fishbone optical model [25] calculations predict that antisymmetrization effects induce an increase of a repulsive potential near the barrier radius as the energy decreases. Furthermore, this effect is predicted to become stronger at negative energies [24]. On the other hand, due to dispersion effects, the interaction is expected to be more attractive in the energy region where the imaginary part of the potential is increasing than at higher energies, and its strength is predicted to decrease again at low energies [26]. A recent analysis [27] of elastic $\alpha + {}^{16}$O scattering data at energies near the Coulomb barrier [9] agrees qualitatively with these theoretical predictions.

Extensive microscopic RGM studies concerning α-cluster states in ^{20}Ne have first been made by Horiuchi and Ikeda [28] who proposed a moleculelike structure for the ground-state rotational band with $K^\pi = 0_1^+$ and the

$K^\pi = 0^-$ excited rotational band with the bandhead at 5.78 MeV. In further investigations [29] it could be shown that the states of the 0^- band have strong α-clustering character. These states belong to a rotational sequence with odd spins ranging from 1 to 9 corresponding to a quantum number $Q = 2N + L = 9$. All the states are resonance states with broad α widths as extracted from α + ^{16}O elastic scattering [4, 8, 11]. On the other hand, the ground-state band with $Q = 8$ is found to have weaker clustering than the $K^\pi = 0^-$ band and to have a transient character between a shell-model-like and a cluster structure. A second positive-parity band in ^{20}Ne with a marked moleculelike structure is the "higher-nodal" $K^\pi = 0_4^+$ band with $Q = 10$. It is composed of very broad states, the first three of which are observed at $E_x \sim 8.3$ MeV (0^+), $E_x \sim 8.8$ MeV (2^+), and $E_x \sim 10.8$ MeV (4^+). The location of the last members of this band is a matter of controversy [30].

The existence of α-cluster states in the ^{19}F nucleus is suggested by experimental results of α-transfer reactions [31–33]. There is a close correspondence between the negative-parity band upon the 0.110 MeV state in ^{19}F ($K^\pi = 1/2_1^-$) and the ground-state band in ^{20}Ne ($Q = 8$) as well as the positive-parity band upon the 5.34 MeV state in ^{19}F ($K^\pi = 1/2_2^+$) and the 0^- band in ^{20}Ne ($Q = 9$). Both the negative- and positive-parity bands are well reproduced by microscopic cluster-model calculations [34, 35] and are found to have a well-developed α-cluster structure.

Buck *et al.* [36, 37] presented a potential model for α-cluster states in ^{20}Ne and ^{19}F. These states are considered as bound states and "single-particle" or potential resonances of a cluster-core potential. The treatment of the potential model is similar to the RGM except that first a different effective potential is used and second the Pauli-exclusion principle is taken into account approximately by the choice of quantum numbers for cluster-core states. The α + ^{16}O potential was obtained [36] by folding the α-cluster and ^{16}O-core nucleon densities using a zero-range nucleon-nucleon (NN) interaction. For the description of α-cluster states in ^{19}F an α + ^{15}N potential with a cosh parametrization is employed [37]. The shape of this potential is very similar to the folding potentials used in Ref. [36]. Applying these α-core potentials, good agreement with energy spectra of the rotational bands, rms radii, $B(E2)$ values, and α-decay widths is obtained. However, in both cases the potentials had not been tested against elastic scattering data. Buck *et al.* emphazise that, in contrast to these results, usual Woods-Saxon potentials with a fixed value of the potential depth V_0 give essentially degenerate or even inverted spectra.

An optical potential description of both α + ^{16}O elastic scattering and α-cluster spectroscopy of the ^{20}Ne nucleus was first given by Michel *et al.* [15]. The global α + ^{16}O optical potential they extracted from elastic scattering data turns out to provide a satisfactory description of the α-cluster structure in ^{20}Ne. The potential locates the $Q = 8, 9, 10$ bands within a few MeV of their experimental counterparts denoted as $K^\pi = 0_1^+, 0^-$, and 0_4^+ rotational bands. Moreover, it predicts electromagnetic intraband transition rates and α widths in good agreement with experimental data.

In the present paper, we give the results of a potential-model calculation which describes in a unified way the α elastic scattering on ^{16}O and ^{15}N in a wide range of energies and the α-cluster states in ^{20}Ne and ^{19}F. The real part of the alpha-nucleus potential is calculated by a double-folding procedure using a realistic effective nucleon-nucleon interaction.

A brief description of the double-folding potential and the dispersion relation approach is given in Sec. II. In Sec. III the results of optical model analyses of elastic scattering data in the range of about 30 to 150 MeV are given. Effective NN interactions with different density dependencies as well as zero-range and finite-range knock-on-exchange potentials are investigated with regard to the quality of the fits. In Sec. IV differential cross sections for α + ^{16}O elastic scattering at energies near the Coulomb barrier are investigated. In Sec. V the results of bound and quasibound state calculations are given. Finally, in Sec. VI the dispersion relation of the optical potential is used to calculate the volume integrals of the real part of the potential. The derived energy dependence of the optical potential is applied to calculate the α + ^{16}O excitation function in an energy range in which strong compound resonances are observed.

II. THEORETICAL CONSIDERATIONS

A. Optical potentials

The microscopic optical potential can be written in a compact form as

$$U(\mathbf{r}, \mathbf{r}'; E) = V_0(\mathbf{r}, \mathbf{r}') + \Delta V(\mathbf{r}, \mathbf{r}'; E) + iW(\mathbf{r}, \mathbf{r}'; E) . \tag{1}$$

This potential is non-Hermitian, strongly energy dependent and nonlocal in coordinate space.

The first term V_0, which we may refer to as the channel potential, is real and represents the average interaction of the colliding nuclei in the absence of nonelastic excitations. It includes exchange terms that arise from antisymmetrization between the two nuclei. Due to these terms V_0 becomes nonlocal, even if the underlying nucleon-nucleon (NN) interaction is assumed to be local.

The remaining term, $\Delta V + iW$, arises from coupling to all other states outside the model space of the elastic channel. This part of the potential is complex, nonlocal, and strongly fluctuating with energy. ΔV is denoted as dynamic polarization potential.

In order to obtain a potential which can be applied in usual numerical calculations, some approximations are necessary. The first one deals with the strong resonances of ΔV which are observed when the incident energy is varied. Some averaging over the energy leads to an averaged potential $\bar{U}(\mathbf{r}, \mathbf{r}'; E)$ which is identified with the nonlocal optical potential [38].

Since most optical potentials used in numerical calculations are taken to be local, $\bar{U}(\mathbf{r}, \mathbf{r}'; E)$ has to be

transformed into an equivalent local potential in a further approximation. This transformation gives rise to an additional energy dependence. Assuming a spherically symmetric shape, the potential can be written as

$$U_{\rm opt}(R;E) = V_0(R;E) + \Delta V(R;E) + iW(R;E) \ . \quad (2)$$

B. The channel potential

The channel potential has the form

$$V_0(R;E) = \langle \psi_P \psi_T | v | \mathcal{A} \psi_P \psi_T \rangle \ . \quad (3)$$

The wave functions ψ_P and ψ_T for the projectile P and the target nucleus T in their ground states are antisymmetrized. Therefore the antisymmetrization operator $\mathcal{A}$ only takes into account the exchange of two nucleons between the two nuclei. This operation splits the channel potential (3) into two parts:

$$V_0(R;E) = \sum_{\substack{i\in P \\ j\in T}} \langle ij|v_d|ij\rangle + \sum_{\substack{i\in P \\ j\in T}} \langle ij|v_{\rm ex}|ji\rangle \ . \quad (4)$$

$|i\rangle$ and $|j\rangle$ refer to the single-particle wave functions of the nucleons in the two nuclei, respectively, v_d is the direct and $v_{\rm ex}$ the exchange part of the NN interaction. These quantities may be described by the four singlet/triplet, even/odd components of the central NN force. Each component has been parametrized by a sum of three Yukawa potentials with parameters adjusted to G-matrix elements of the Reid [39] or the Paris [40] NN interaction. The resulting parameters of the so-called M3Y interaction are given in Ref. [41].

A first and commonly used procedure in calculating the exchange part in (4) is the choice of a δ function for the interaction $v_{\rm ex}$ which is scaled by an energy-dependent strength function $J_{00}(E)$ [42]:

$$J_{00}(E) = -276(1 - 0.005E/A_P) \ \text{MeV fm}^3. \quad (5)$$

E/A_P is the energy per nucleon of the projectile. Applying this approximation, the expression for the channel potential is reduced to one term:

$$V_0(R;E) = \int_0^\infty \int_0^\infty \rho_T(\boldsymbol{\xi}_i)\rho_P(\boldsymbol{\xi}_j) g(E,|\mathbf{s}|) d\boldsymbol{\xi}_i d\boldsymbol{\xi}_j \quad (6)$$

with

$$g(E,|\mathbf{s}|) = 7999\frac{\exp(-4s)}{4s} - 2134\frac{\exp(-2.5s)}{2.5s} + J_{00}(E)\delta(\mathbf{s}) \ . \quad (7)$$

The geometrical quantities R, $\boldsymbol{\xi}_i$, $\boldsymbol{\xi}_j$ and $\mathbf{s}$ are shown in Fig. 1. Kobos *et al.* [17] have modified the M3Y interaction by introducing a density- and energy-dependent term which has the form

$$t(E,\rho,s) = g(E,|\mathbf{s}|) f(E,\rho) \ . \quad (8)$$

The density-dependent term $f(E,\rho)$ was chosen as

$$f(E,\rho) = C(E)[1 + \alpha(E) e^{-\beta(E)\rho}] \quad (9)$$

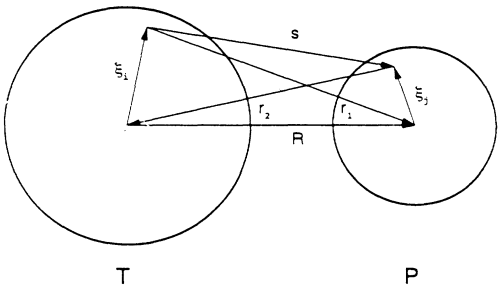

FIG. 1. Geometric parameters for the double-folding potential.

with $\rho = \rho_T(\boldsymbol{\xi}_i) + \rho_P(\boldsymbol{\xi}_j)$. The parameters $C(E)$, $\alpha(E)$, and $\beta(E)$ were determined by fitting the volume integral of $t(E,\rho,s)$ to the strength of the real part of a G-matrix effective interaction obtained from Brueckner-Hartree-Fock calculations [43] for nuclear matter of various densities ρ and at various energies. The form (8) implies that the exchange term is also density dependent. The effective interaction (8) folded with the nuclear densities gives realistic double-folded alpha-nucleus potentials [16, 17]:

$$V_F(R;E) = \int_0^\infty \int_0^\infty \rho_T(\boldsymbol{\xi}_i)\rho_P(\boldsymbol{\xi}_j) t(E,\rho,s) d\boldsymbol{\xi}_i d\boldsymbol{\xi}_j \ . \quad (10)$$

Another ansatz for the density dependence is expressed by the form [44]

$$f(\rho) = (1 - \beta\hat{\rho}^\nu)/(1 - \beta/2^\nu) \ . \quad (11)$$

β denotes the strength parameter and $\hat{\rho} = \rho/\rho_0$ is the density normalized to the nuclear matter value $\rho_0 = 0.17$ fm^{-3}. The factor $(1 - \beta/2^\nu)^{-1}$ ensures that $f(\rho) = 1$ for $\rho = \rho_0/2$, where the M3Y interaction is valid. Ermer *et al.* [44] find good agreement between elastic proton, deuteron, and α-particle scattering data on ^{40}Ca and ^{208}Pb at 26–30 MeV/A_P and the results of calculations using density parameters $\nu = 1/3$ and $\beta = 0.47$.

A further possibility to calculate the exchange term is based on the density matrix formalism [41, 45–47]. Khoa *et al.* [46, 47] obtained a closed expression for $V_{\rm ex}(R;E)$ in Eq. (4). This model reproduces some α and heavy-ion scattering data with good accuracy. In our calculations, presented in Sec. III, we have modified the expression of this finite-range exchange term by introducing the density-dependent term $f(E,\rho)$ [Eq. (9)] into the exchange term [48]. As a result we get similar but density-dependent expressions as those given by Khoa *et al.* [47].

C. Dispersion relations

According to the causality principle, which states that a scattered wave cannot be emitted before the interaction has occurred, a dispersion relation between ΔV and W of Eq. (1) exists. As shown by Mahaux, Ngo, and Satchler [26] and recently by Pacheco *et al.* [49] this dis-

persion relation also holds in good approximation for the corresponding terms of the equivalent local potential Eq. (2) and can be written

$$\Delta V(R;E) = \frac{\mathcal{P}}{\pi}\int_0^\infty \frac{W(R;E')}{E'-E}dE' \quad (12)$$

with $\mathcal{P}$ denoting the Cauchy principal value.

The strength of an interacting potential $U(E)$ between a projectile P and a target nucleus T can be measured by its volume integral per interacting pair of nucleons

$$J_U(E) = \frac{4\pi}{A_P A_T}\int_0^\infty U(r,E)r^2dr \quad (13)$$

where A_P and A_T denote the projectile and target mass numbers, respectively. From Eq. (12) it follows that a similar dispersion relation holds for the volume integrals $J_{\Delta V}(E)$ and $J_W(E)$, namely,

$$J_{\Delta V}(E) = \frac{\mathcal{P}}{\pi}\int_0^\infty \frac{J_W(E')}{E'-E}dE' \, . \quad (14)$$

Since the real part of the optical potential [Eq. (2)] is composed of two terms, $V(R;E) = V_0(R;E)+\Delta V(R;E)$, one has to distinguish between the energy dependence of $J_{V_0}(E)$, which is calculated by one of the folding procedures, and the energy dependence of $J_{\Delta V}(E)$, which is related to that of the imaginary part $J_W(E)$ by the dispersion relation (14).

Due to the difficulties in the calculation of the absolute dispersion relation [Eq. (14)] in the nucleus-nucleus case, we use in our calculations the "subtracted dispersion relation" [26]:

$$J_{\Delta V}(E) - J_{\Delta V}(E_s)$$

$$= (E-E_s)\frac{\mathcal{P}}{\pi}\int_{E_0}^\infty \frac{J_W(E')}{(E'-E_s)(E'-E)}dE' \, . \quad (15)$$

E_s is a reference energy which lies in the energy domain of interest. Little is known about the energy behavior of the imaginary part of α-nucleus optical potentials for α energies higher than about 200 MeV. Therefore an appropriate choice of E_s lies in between about 30 and 100 MeV. The lower limit of the integral (15) is taken close to the smallest of the bound state energies E_0 of the colliding system $P+T$.

III. DIFFERENTIAL CROSS SECTIONS IN THE RANGE 30-150 MEV

First we consider the description of the elastic α scattering on ^{16}O and ^{15}N in the optical model (OM). The experimental data are taken from Refs. [10, 12, 15, 16, 50–57], they are shown together with the results of the OM calculations in Figs. 2 and 3.

The optical potential used has the form

$$U_{\rm opt}(r,E) = V_C(r,E) + \lambda_R V_F(r,E) + i\, W(r,E) \, . \quad (16)$$

For the Coulomb term $V_C(r,E)$ the potential of a uniformly charged sphere was assumed using a radius parameter $r_c = 1.25$ fm. The real term $V_F(r,E)$ is given by Eq. (10). The normalization factor λ_R is a free parameter in the fitting procedure. The choice of an optical potential according to Eq. (16) implies that the same radial shape is assumed for both the channel potential $V_0(R;E)$ and the dispersive contributions to the real potential, $\Delta V(R;E)$, as given by Eq. (2), and that the latter term is taken into account by the multiplication of the folding potential V_F with the scaling factor λ_R.

The exchange part of the folding potential has been calculated in its zero-range version as outlined in Sec. II B. For the density dependence of the effective NN interaction, the expression of Kobos *et al.* [17] [Eq. (9)] was used. The parameters $C(E)$, $\alpha(E)$, and $\beta(E)$ were determined by the method described in Sec. II B. The resulting values are very close to those given in Ref. [17]. For the point-nucleon densities of the α particle and of ^{15}N and ^{16}O, experimentally known charge distributions [58] with different parametrizations are used. As all combinations of differently parametrized distributions give similar re-

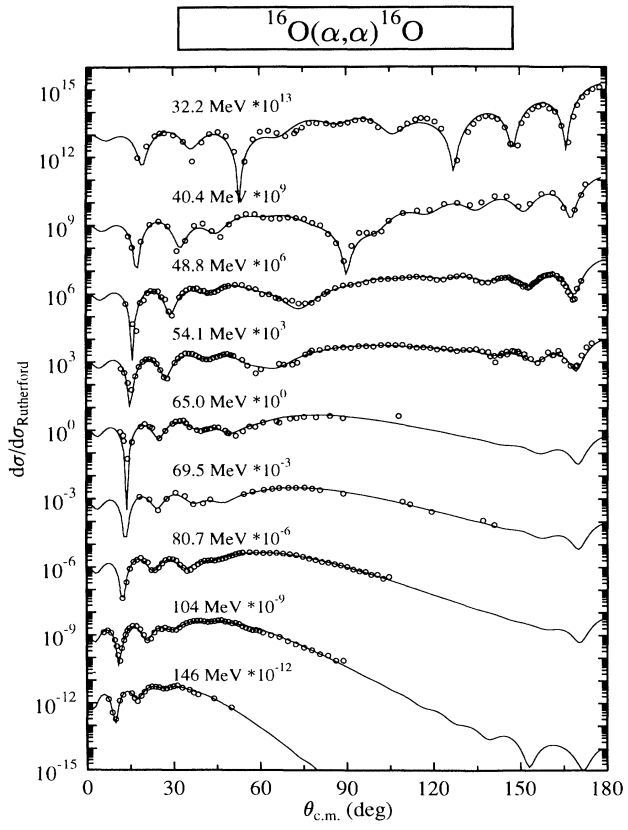

FIG. 2. Elastic α scattering on ^{16}O: Experimental data and optical model fits, calculated by using double-folding potentials, at incident energies 32.2 MeV [10], 40.4 MeV [50], 48.8 and 54.1 MeV [16], 65.0 MeV [55], 69.5 MeV [15], 80.1 MeV [52], 104 MeV [53], and 146 MeV [54]. (The 104 MeV data have been multiplied by 0.729 [15].)

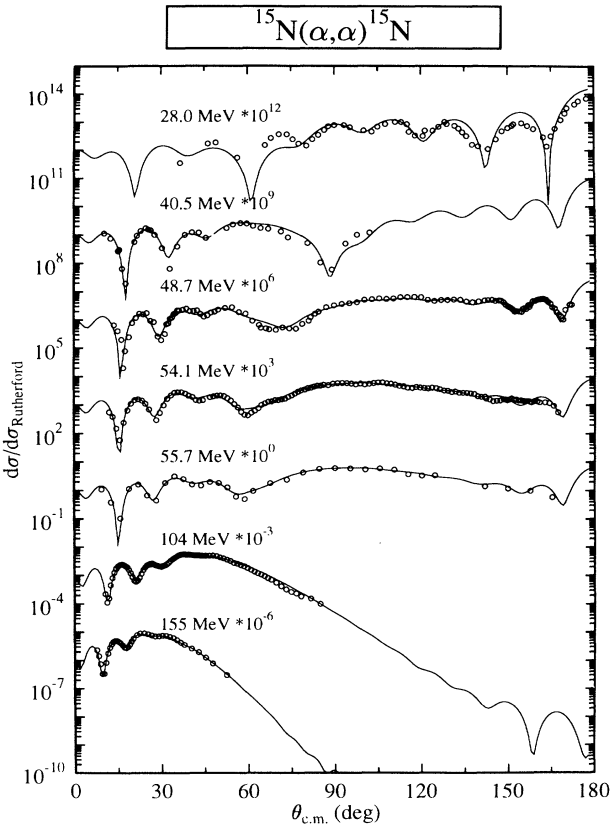

FIG. 3. Elastic α scattering on ^{15}N: Experimental data and optical model fits calculated by using double-folding potentials, at incident energies 28.0 MeV [12], 40.5 MeV [55], 48.8 and 54.1 MeV [16], 55.7 MeV [50], 104 MeV [56], and 155 MeV [57].

sults in the folding calculations, only those based on the parametrization by a sum of Gaussians (SOG) for both, α particle and target nuclei, are shown in the figures.

For the imaginary part we likewise chose the shape of a double-folded potential multiplied with a scaling factor λ_I which allows one to adjust the depth of the potential:

$$W(rE) = -10\lambda_I \int\int \rho_T(\xi_i)\rho_P(\xi_j)\delta(\mathbf{r} - \boldsymbol{\xi}_i + \boldsymbol{\xi}_j) \times d\boldsymbol{\xi}_i d\boldsymbol{\xi}_j \ . \quad (17)$$

In order to alter the width of the potential a spreading factor κ_I as a second free parameter of the imaginary potential is used which transforms the radial coordinate r to $\kappa_I r$.

All fits were performed using the computer code GOMPF [59]. As shown in Figs. 2 and 3, for the whole energy range a good agreement between experimental and calculated data has been found. The normalization factors λ_R and λ_I, the spreading factor κ_I, and the integral potential parameters obtained in this analysis are listed in Table I. The real and imaginary parts of the optical potentials derived are shown in Fig. 4. The required normalization factors λ_R are close to the values obtained in previous analyses [16, 17]. As already mentioned by Kobos *et al.* [17], the departures of λ_R from unity indicate a deficiency in the normalization of the model interaction as defined by Eqs. (5) – (9) and by the fit of the parameters $C(E)$, $\alpha(E)$, and $\beta(E)$ in Eq. (9) to the results of Jeukenne *et al.* [43]. Furthermore, the dispersive contributions to the real potential are likewise taken into account by the normalization factor λ_R. In a further analysis of the α + ^{16}O data, the exchange part of the folding potential has been calculated in finite-range approximation as outlined in Sec. II B. We solve the exchange integral by iteration of each radial point to ensure

TABLE I. Normalization factors λ_R for the real part, normalization factors λ_I, and scaling factors κ_I for the imaginary part of the double-folding potential as well as volume integrals and rms radii for the optical-model analysis of elastic α scattering on ^{16}O and ^{15}N.

	E_α^{lab} (MeV)	λ_R	J_R (MeV fm^3)	$\langle r_R^2\rangle^{1/2}$ (fm)	λ_I	κ_I	J_I (MeV fm^3)	$\langle r_I^2\rangle^{1/2}$ (fm)
^{16}O +α	32.2	1.375	399.6	3.601	1.708	1.328	40.00	3.951
	40.45	1.357	389.9	3.602	2.157	1.368	55.12	4.069
	48.7	1.367	388.8	3.604	2.660	1.383	70.29	4.114
	54.1	1.351	381.1	3.605	2.795	1.391	75.13	4.137
	65.0	1.343	370.7	3.607	3.104	1.409	86.88	4.192
	69.5	1.309	361.4	3.607	3.186	1.407	88.66	4.185
	80.7	1.300	353.2	3.610	3.427	1.415	96.99	4.208
	104.0	1.252	328.2	3.615	3.609	1.426	104.54	4.238
	146.0	1.236	302.2	3.628	3.667	1.435	108.28	4.264
^{15}N +α	28.0	1.420	404.2	3.584	1.511	1.312	34.10	3.864
	40.6	1.410	400.8	3.586	2.311	1.369	59.30	4.003
	48.7	1.416	394.6	3.591	2.664	1.389	71.30	4.090
	54.1	1.380	385.3	3.587	3.027	1.394	81.87	4.106
	55.7	1.379	384.0	3.587	3.030	1.394	82.02	4.107
	104.0	1.266	328.7	3.597	3.560	1.426	103.12	4.198
	155.0	1.266	302.2	3.613	3.640	1.436	107.67	4.226

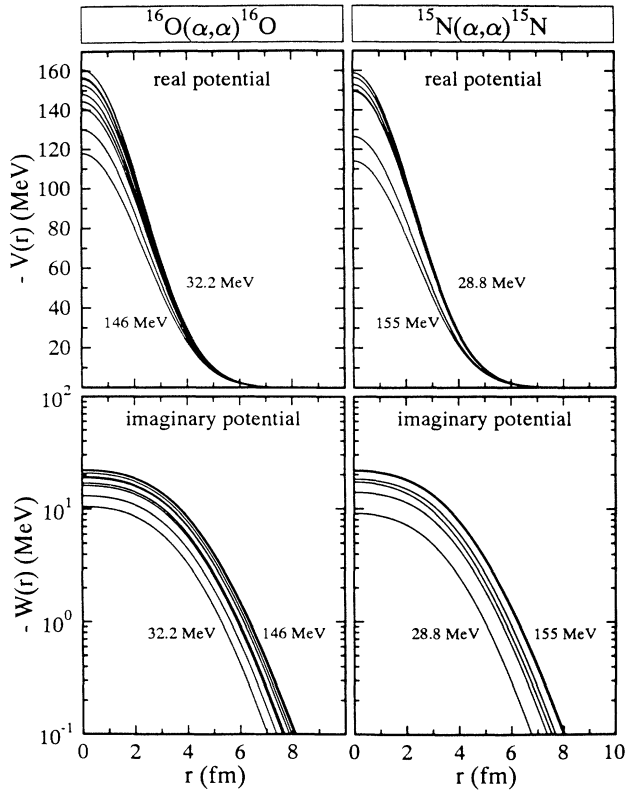

FIG. 4. Real and imaginary parts of the α + ^{16}O and α + ^{15}N optical potential used in the calculations shown in Figs. 2 and 3. The imaginary part is given in a logarithmic scale.

self-consistency. The numerical details of this procedure are given in Ref. [48]. In order to test the influence of the density dependence (DD) of the NN interaction to the quality of the fits, we calculate the channel potential not only with the Kobos type [Eq. (9)] but also with the Ermer type [Eq. (11)] DD function.

In this way, four kinds of calculations have been carried out using either zero-range (ZRE) or finite-range (FRE) exchange terms and using the Kobos type (KDD) as well as the Ermer type (TDD) of density dependence. To be more flexible in the calculations we have used imaginary potentials of surface Woods-Saxon shape in this analysis. Again we adjust the volume integral of the channel potential and the three parameters of the surface Woods-Saxon imaginary potential by fitting the calculated to the experimental scattering data. For energies of E_α = 48.7 and 54.1 MeV the results are shown in Fig. 5, the potentials are given in Fig. 6, and the rms radii, the volume integrals, and the parameters of the potentials used are listed in Table II.

The rms radii and the depths of the real potentials are somewhat larger in the FRE than in the ZRE calculations (about 1% and 6%, respectively) whereas for each energy the quality of the fits is comparable for both kinds of calculation. Concluding these results, one can state that both approximations in localizing the exchange part of the channel potential, namely the localization of the interaction (ZRE) or the localization of the nuclear densities (FRE), in combination with the chosen effective NN interaction yield a good description for the system α + ^{16}O.

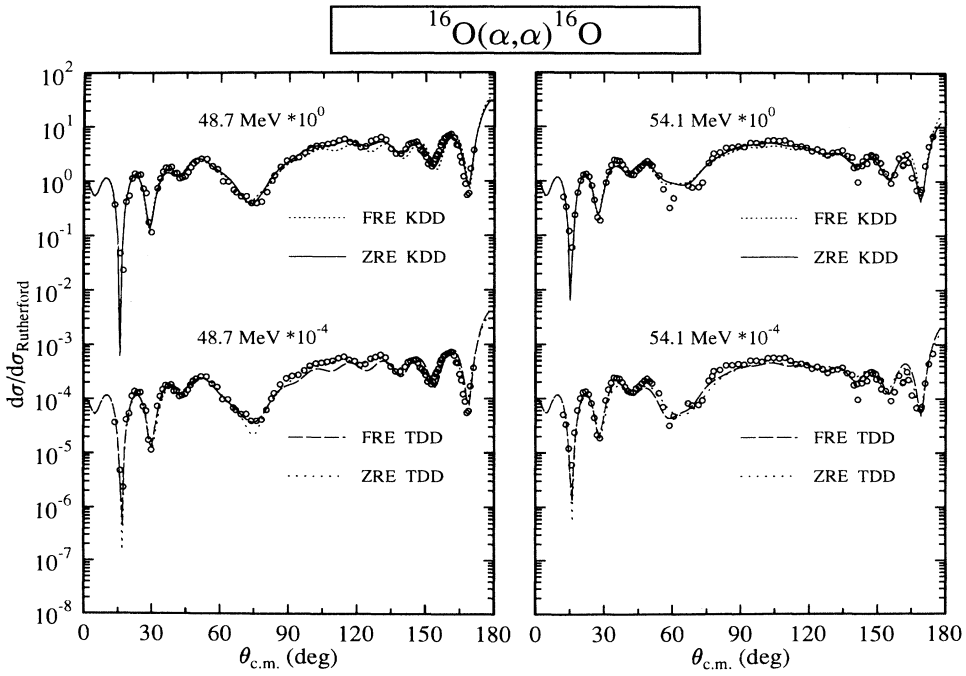

FIG. 5. Elastic α scattering on ^{16}O: Experimental data [16] and optical-model fits using zero-range (ZRE) and finite-range (FRE) exchange terms and the Kobos type (KDD) as well as the Ermer type (TDD) of density dependence in the NN interactions.

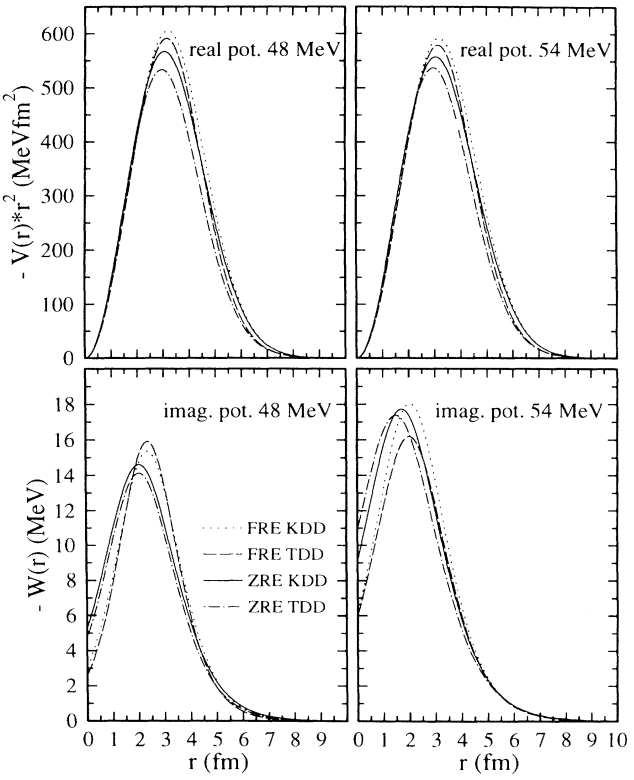

FIG. 6. Real and imaginary parts of the α + ^{16}O optical potentials used in the calculations shown in Fig. 5.

As a tendency we find that the potentials calculated with the TDD are somewhat smaller in depth and width than those calculated with a KDD. But the variation of the real part of the potential is compensated by a variation of its imaginary part, thus resulting in very similar S-matrix elements for each energy. Summarizing these results, we find that the description of the experimental data is satisfactory for all combinations of exchange and DD terms.

As a practical result of these studies we conclude that it is sufficient to use the numerically most convenient form of the double-folding integral which is given by a ZRE-type exchange and a Kobos-type DD term. Therefore all analyses described in the next sections are carried out using this form of the folding potential.

IV. DIFFERENTIAL CROSS SECTIONS FOR α + ^{16}O ELASTIC SCATTERING AT ENERGIES NEAR THE COULOMB BARRIER

At low energies differential cross sections for α + ^{16}O elastic scattering were measured by Buser [9] at eleven energies between $E_\alpha = 3.485$ and 4.878 MeV. The energies are close to the Coulomb barrier ($E_{\rm CB} \simeq 3$ MeV) and they are lower than the energy of the first inelastic threshold. In the energy range covered by these data McDermott *et al.* [2] have measured excitation functions. A phase-shift analysis resulted in the discovery of two broad overlapping $J^\pi = 0^+$ and 2^+ resonances in this region. Using RGM calculations [29] these states are identified as the first two members of the second positive-parity band in ^{20}Ne ($K^\pi = 0^+_4$) which is marked by a significant moleculelike $\alpha \otimes {}^{16}$O cluster structure.

The experimental data of Buser are shown in Fig. 7 together with data at 5.2, 5.5, 5.8, and 6.2 MeV measured by John *et al.* [5]. We have reanalyzed these data in an OM calculation using a real potential of the form

$$U_{\rm opt} = V_c(r) + \lambda_R V_F(r, E) \; . \tag{18}$$

Both, the Coulomb and the nuclear part of the potential were calculated by a double-folding procedure. In the calculation of the nuclear potential the zero-range exchange term [Eq. (5)] and the expression of Kobos *et al.* [Eq. (9)] for the density dependence of the effective NN interaction were applied. For the nucleon densities of the ^{16}O nucleus and the α particle, values given in the SOG parametrization were used [58].

In a first attempt we tried to fit the data with a unique but energy-dependent normalization factor $\lambda_R(E)$. The results of this one-parameter fit are shown in Fig. 7 as dashed lines, the factors $\lambda_R(E)$ and the volume integrals of the nuclear potentials are listed in Table III. The calculations reproduce the trends of the experimental cross section values fairly well, but in some details the agreement between the two sets of data is poor, especially at backward angles and in the regions of the cross section minima. This means that at energies near the Coulomb

TABLE II. Normalization factors λ_R of the double-folding potential for the real interaction as well as volume integrals and rms radii for the optical-model analysis of the elastic α-^{16}O scattering at $E_\alpha = 48.7$ and 54.1 MeV using different combinations of exchange and DD terms in the double-folding potential.

$E_\alpha^{\rm lab}$ (MeV)	Density dependence	Exchange term	λ	J_R (MeV fm^3)	$\langle r_R^2\rangle^{1/2}$ (fm)	J_I (MeV fm^3)	$\langle r_I^2\rangle^{1/2}$ (fm)
48.7	KDD	ZRE	1.357	386.1	3.604	71.72	4.141
		FRE	1.364	404.7	3.648	75.96	4.003
	TDD	ZRE	0.934	352.4	3.476	64.96	4.033
		FRE	0.999	379.5	3.550	70.89	3.838
54.1	KDD	ZRE	1.345	379.5	3.605	78.87	4.168
		FRE	1.354	395.8	3.650	83.73	4.056
	TDD	ZRE	0.933	350.9	3.478	74.22	4.239
		FRE	0.986	371.8	3.552	77.45	4.100

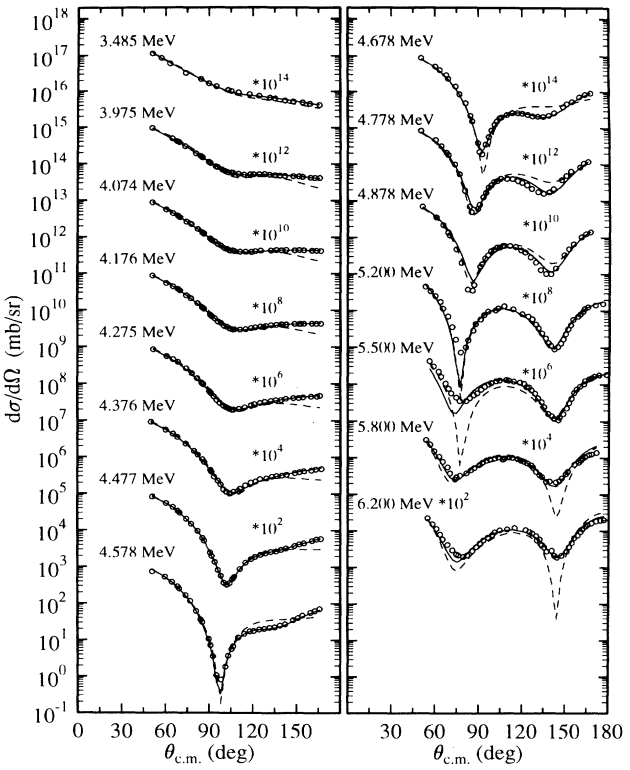

FIG. 7. Elastic α scattering on ^{16}O: Experimental values [5,9] and optical-model fits calculated by using L-independent (dashed lines) and L-dependent (full lines) double-folding potentials.

barrier the assumption of a local potential is too simple to describe the data. A similar resume has already been given by Michel *et al.* [27].

Due to these difficulties, in a second attempt L-dependent potentials are applied. In a first step we use two sets of folding potentials at each energy characterized by their normalization factors $\lambda_R^{L=0}$ and $\lambda_R^{L\geq 1}$ whereas in a second step three parameters, $\lambda_R^{L=0}$, $\lambda_R^{L=2}$, and $\lambda_R^{L=1,\geq 3}$, are allowed. The normalization factors resulting from the fit procedure are listed in Table III. Since the folding potential V_F is assumed to be energy independent in the energy range considered, the volume integrals of the nuclear potentials are given as the product of λ_R with $J_R(V_F) = 298.7$ MeV fm^3. The normalization factors obtained in the two-parameter fits are very similar to the corresponding λ_R values of the three-parameter fits. Consequently for each energy the two cross section curves are nearly indistinguishable from each other and therefore the full lines in Fig. 7 represent the results of both the two- and three-parameter fits. Now the description of the experimental data is obviously of much better quality than that of the first attempt using an L-independent folding potential.

This improvement can be attributed to the potential for the $L = 0$ partial waves, which turns out to be somewhat shallower than the potential for the other partial waves (see Table III). The relative difference in the depths decreases with increasing energy, namely from about 6% (at $E_\alpha = 3.485$ MeV) to about 1.5% (at $E_\alpha = 4.878$ MeV). For the four higher energies 5.2, 5.5, 5.8, and 6.2 MeV the results are nonuniform. This may be caused by some resonances in this region; the effects of those are not taken into account in the present analysis.

The phase shifts for the $L = 0$ and $L = 2$ partial waves obtained from the three optical model fits to the angular distributions are shown in Fig. 8 together with the results of McDermott *et al.* [2] mentioned above. There is a good agreement between the results of both types of analyses. The energies at which δ_0 and δ_2 cross 90° are near 4.8 and 5.1 MeV, corresponding to $E_x \approx 8.6$ and 8.8 MeV, respectively.

Michel *et al.* [27] have analyzed the same data set within a local-potential model approach, too. They find that these data can be described very accurately using a

TABLE III. Normalization factor λ_R and volume integrals of the double-folding potential used in the optical-model analysis of elastic α scattering on ^{16}O.

	One-parameter fit		Two-parameter fit		Three-parameter fit		
$E_\alpha^{\rm lab}$ (MeV)	λ_R	J_R (MeV fm^3)	$\lambda_R^{L=0}$	$\lambda_R^{L\geq 1}$	$\lambda_R^{L=0}$	$\lambda_R^{L=2}$	$\lambda_R^{L=1,\geq 3}$
3.485	1.280	382.5	1.204	1.279	1.204	1.279	1.279
3.975	1.263	377.2	1.221	1.286	1.221	1.286	1.285
4.074	1.265	377.8	1.243	1.308	1.242	1.308	1.300
4.176	1.267	378.6	1.253	1.315	1.252	1.313	1.301
4.275	1.278	381.8	1.259	1.320	1.258	1.318	1.291
4.376	1.290	385.3	1.269	1.321	1.268	1.320	1.291
4.477	1.301	388.7	1.276	1.328	1.274	1.327	1.293
4.578	1.313	392.1	1.299	1.332	1.297	1.332	1.322
4.678	1.322	394.9	1.305	1.335	1.299	1.337	1.326
4.778	1.333	398.2	1.316	1.337	1.303	1.341	1.327
4.878	1.334	398.5	1.318	1.334	1.306	1.341	1.327
5.2	1.342	400.9	1.348	1.343	1.354	1.334	1.322
5.5	1.329	396.8	1.442	1.348	1.349	1.323	1.297
5.8	1.387	414.4	1.531	1.343	1.336	1.367	1.293
6.2	1.365	407.7	1.511	1.331	1.517	1.329	1.317

potential providing (i) this interaction is made slightly L dependent and (ii) its diffuseness is significantly reduced with respect to that needed at higher energies. This second feature results in an increase of a repulsive potential near the nuclear surface with decreasing energy in agreement with recent theoretical predictions as mentioned in the introduction [23–26].

Concluding our results we find that these data can also be described very accurately using a double-folded potential whose depth is somewhat smaller than that needed at higher energies. This potential has likewise to be made slightly L dependent, but unlike Michel *et al.* [27] it is of the same shape and therefore has the same rms radius with respect to that used at higher energies. That means that due to the double-folding procedure in calculating the potential a possibly existing potential barrier near the nuclear surface cannot be found. From our point of view the results of the present analysis can be interpreted in the way that the low energy scattering data can be described thoroughly without any additional potential barrier.

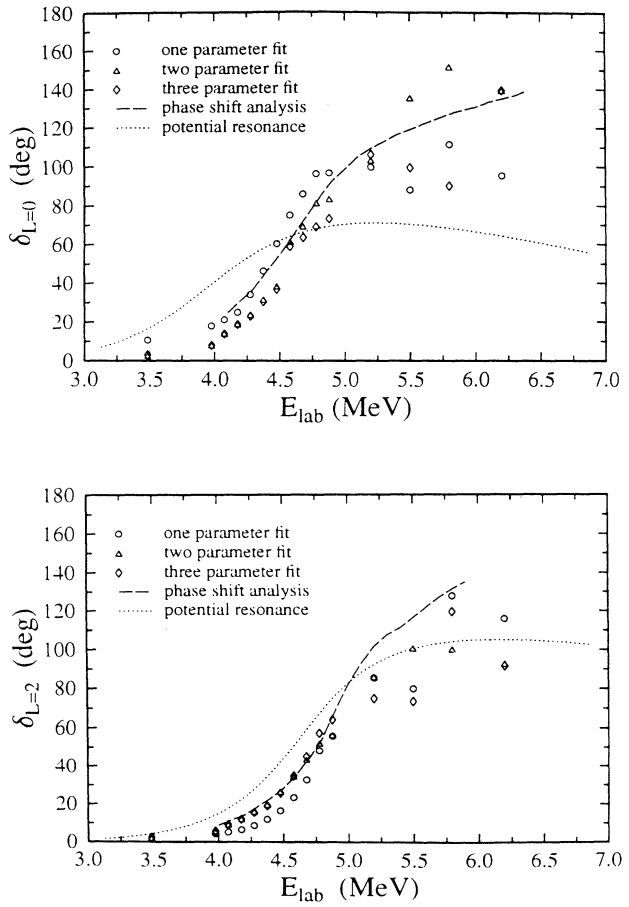

FIG. 8. Phase shifts $\delta_{L=0}$ and $\delta_{L=2}$ obtained from optical-model fits shown in Fig. 7 (open symbols) together with the results of a phase-shift analysis [2] (dashed lines) as well as a quasibound state calculation (dotted lines) (see text in Sec. V).

V. BOUND STATES AND POTENTIAL RESONANCES

As a next step we use the double-folding α-nucleus potential as a suitable cluster-core potential and calculate bound states and single-particle (single-cluster) resonances. The wave function $u_{NL}(r)$ which describes the relative motion of the α-nucleus system is characterized by the node number N and the orbital angular momentum number L. These N and L values are related to the corresponding quantum numbers n_i and l_i of the four nucleons forming the α cluster:

$$Q = 2N + L = \sum_{i=1}^{4} 2n_i + l_i = \sum_{i=1}^{4} q_i \,. \tag{19}$$

Thus for $^{20}\mathrm{Ne} = \alpha \otimes {}^{16}\mathrm{O}$ one expects five cluster states for the ground state ($K^\pi = 0_1^+$) band and five states for the first negative-parity ($K^\pi = 0^-$) band with $Q = 8$ and 9, respectively. For the "higher-nodal" ($K^\pi = 0_4^+$) band six states are expected with $Q = 10$. Since the ^{15}N ground state largely can be represented by a $p_{1/2}$ hole in the closed $1p$ shell, the states of the $K^\pi = 0_1^+$ band in ^{20}Ne correspond to the states of the $K^\pi = 1/2_1^-$ band in ^{19}F, and the states of the $K^\pi = 0^-$ band in ^{20}Ne with those of the $K^\pi = 1/2_2^+$ band in ^{19}F. The $\alpha \otimes {}^{15}$N cluster states split in close doublets because of the small spin-orbit potential resulting from the motion of the massive ^{15}N nucleus in the field of the α particle.

In the calculations of the cluster states in the framework of our folding-potential model (FPM) we first fixed the depth of the potentials that the computed excitation energies of the states considered coincide with their experimental values. For the ^{20}Ne nucleus we analyzed the states of the ground-state band, the $K^\pi = 0^-$ band, and the first two members of the higher-nodal band. For ^{19}F we calculated the L centroids of the states of the $K^\pi = 1/2_1^-$ band and $K^\pi = 1/2_2^+$ band. The results of this calculation are listed in Table IV. The potentials obtained are very close to each other and to those deduced from the optical-model analysis of the α + ^{16}O cross section data at low energies (see Table III). In a second step the excitation energies of the bound and resonance states of four rotational bands were calculated applying for each band the potential deduced for its bandhead. The resulting level schemes are shown in Fig. 9, together with the experimental values [60] and the results of microscopic calculations [21,35]. The energy splittings both in ^{20}Ne and ^{19}F are well reproduced by our calculations, except for the $L = 8$ states in both nuclei and the $L = 7$ and $L = 9$ states in ^{20}Ne. The calculated states lie very close to an ideal $L(L+1)$ rotational spectrum, while the experimental $L = 7, 8$, and 9 states deviate strongly from this rule. For the $L = 8$ states this behavior is well known [15, 36, 37]. In the case of the $L = 7$ and $L = 9$ states in ^{20}Ne, the levels at $E_x = 15.34$ and 22.87 MeV are assigned as members of the 0^- band [61], marked in Fig. 9 as dotted lines and given in Table IV in parentheses. But in Ref. [60] the states at $E_x = 13.69$ and 17.43 MeV are characterized as the highest members of the 0^- band.

With this assignment the agreement between experimental and calculated results is poor. Therefore we suggest that the older assignment is the correct one.

McArthur *et al.* [8] have measured the yield curves for α particles scattered on ^{16}O at $\Theta_{\text{c.m.}} = 160°$ for the first two members of the $K^\pi = 0^-$ band in ^{20}Ne. Using the potentials which localize the exact resonance energies of the two states (Table IV) we have calculated excitation functions at $\Theta_{\text{c.m.}} = 160°$ in the vicinity of the resonance energies. The results are shown together with the experimental data in Fig. 10. Both resonances are well described by the double-folding potential meaning that the term "potential resonance" is justified.

Furthermore, we have calculated the phase shifts in the range of the two broad 0^+ and 2^+ resonances of the higher-nodal band in ^{20}Ne using the appropriate potentials which yield the resonance energies at $E_x = 8.7$ and 8.8 MeV [60], respectively. The results are shown in Fig. 8 as dotted lines. The poor agreement between the results of this calculation and the results of both the phase-shift analysis of McDermott *et al.* [2] and our optical-model analysis of the elastic scattering data of Buser [9] may be caused by the strong energy dependence of the strength of the optical potential in this energy range: In contrast to our analysis of the elastic scattering data, we have used in the phase-shift calculation over the range of each broad resonance the same normalization factor λ_R which has been fixed by the value of the excitation energy $E_x \approx 8.7$ and 8.8 MeV, respectively.

Further information about the quality of the α-cluster potentials can be obtained by the calculation of electromagnetic transition rates between the levels of a rotational band. In a cluster-core model the $B(E2)$ values for a transition $L' = L + 2 \rightarrow L$ are given by

$$B(E2) = \frac{16}{5\pi}[u_{N,L+2}(r)|e_{\text{eff}}r^2|u_{N,L}(r)]^2(L'020|L0)^2 \ . \tag{20}$$

We calculated $B(E2)$ values for the transitions between the states of the ground-state band and between the 3^- and the 1^- state of the $K^\pi = 0^-$ band in ^{20}Ne, which can be compared with experimental [60, 62] and shell-model [36] values. The results are listed in Table V. In our calculation we do not use an effective charge and put

TABLE IV. Normalization factors λ and volume integrals J_R of the double-folding potentials obtained in the analysis of the bound and quasibound α-cluster states in ^{20}Ne and ^{19}F.

	E_x [a] (MeV)	$E_\alpha^{\text{c.m.}}$ (MeV)	K^π	J^π	L_α	Q	λ_R	J_R (MeV fm^3)
^{20}Ne	g.s.	-4.73	0_1^+	0^+	0	8	1.237	370.9
	1.63	-3.10		2^+	2		1.220	365.7
	4.25	-0.48		4^+	4		1.212	363.4
	8.78	4.05		6^+	6		1.200	357.4
	11.95	7.22		8^+	8		1.265	375.1
	5.79	1.05	0^-	1^-	1	9	1.267	378.4
	7.16	2.43		3^-	3		1.277	381.4
	10.26	5.53		5^-	5		1.279	380.2
	13.69	8.96		7^-	7		1.321	394.2
	(15.34 [b]	10.61		7^-	7		1.274	375.7)
	17.43	12.70		9^-	9		1.405	419.7
	(22.87 [b]	18.14		9^-	9		1.296	366.6)
	~ 8.7	3.97	0_4^+	0^+	0	10	1.302	388.7
	~ 8.8	4.07		2^+	2		1.351	402.4
^{19}F	0.11	-3.90	$1/2_1^-$	$1/2^-$	0	8	1.283	379.7
	1.35	-2.67		$5/2^-$	2		1.275	377.5
	1.46	-2.56		$3/2^-$				
	4.00	-0.02		$7/2^-$	4		1.271	376.1
	4.03	0.02		$9/2^-$				
	8.29	4.27		$13/2^-$	6		1.253	371.0
	8.95	4.94		$11/2^-$				
	12.26 [c]	8.25		$17/2^-$	8		1.309	387.5
	12.65 [c]	8.64		$15/2^-$				
	5.34	1.33	$1/2_2^+$	$1/2^+$	1	9	1.301	387.4
	5.50	1.49		$3/2^+$				
	6.28	2.27		$5/2^+$	3		1.323	391.7
	7.11	3.10		$7/2^+$				
	9.93	5.91		$9/2^+$	5		1.314	389.1
	10.37	6.35		$11/2^+$				

[a] Reference [60].
[b] Reference [61].
[c] Reference [33].

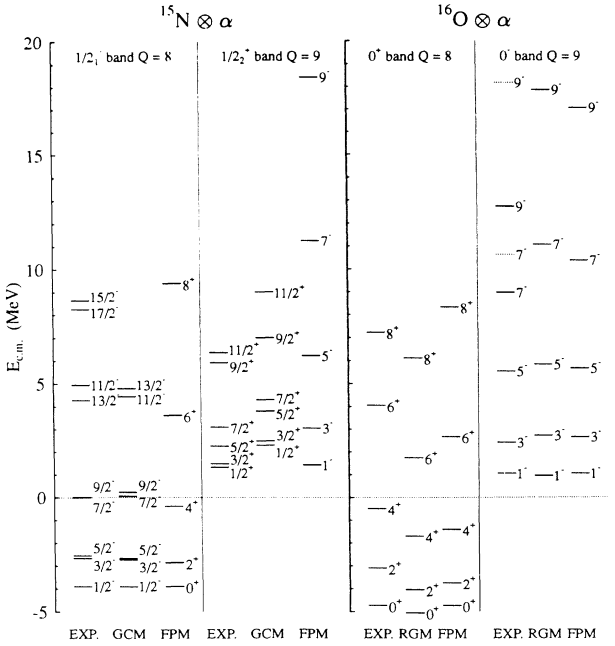

FIG. 9. Experimental level scheme for the $Q = 8$ and $Q = 9$ rotational bands in ^{19}F and ^{20}Ne [60] together with the results of RGM [21, 35] and our folding-potential model (FPM) calculations. The experimental $L = 7$ and $L = 9$ levels in ^{20}Ne, shown as dotted lines, are taken from Ref. [61].

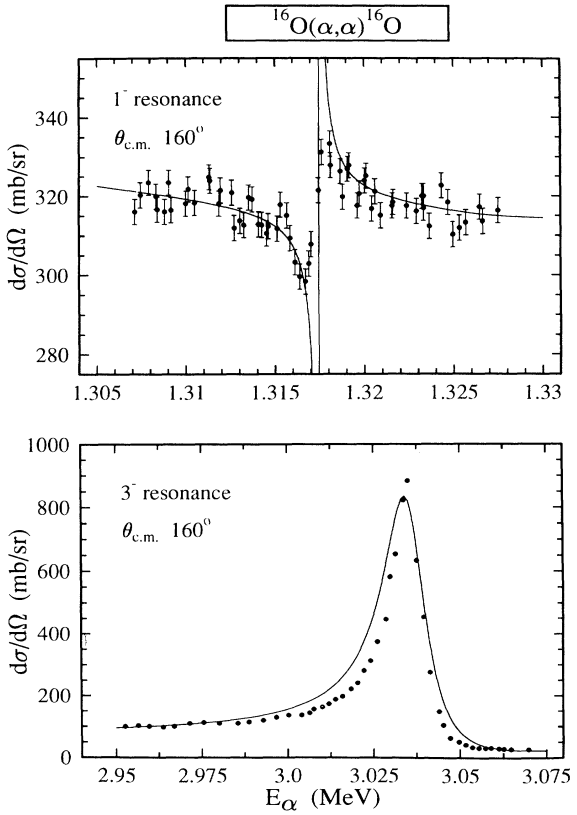

FIG. 10. Elastic scattering of α particles at $\Theta_{c.m.} = 160°$ near the 1^- and 3^- resonances in ^{20}Ne. Comparison of the experimental values [8] with the results of our optical-model analysis.

TABLE V. $B(E2)$ values in $e^2\,fm^4$ for the transitions between the states of the g.s. band and the first two members of the $K^\pi = 0^-$ band in ^{20}Ne.

	Expt. values a	Expt. values b	Shell model [c]	This work
$2_1^+ \rightarrow 0_1^+$	65.5 ± 3.2	58.1 ± 6.5	52.6	50.8
$4_1^+ \rightarrow 2_1^+$	70.9 ± 6.5	67.7 ± 6.5	64.5	68.3
$6_1^+ \rightarrow 4_1^+$	64.4 ± 9.7	64.5 ± 9.7	53.4	54.5
$8_1^+ \rightarrow 6_1^+$	29.1 ± 4.2		32.8	31.2
$3^- \rightarrow 1^-$	161.3 ± 25.8			157.0

[a]Reference [60].
[b]Reference [62].
[c]Reference [36].

$e_{eff} = e$. Comparing the data a good agreement is found.

As a further test of our simple cluster model we calculate the charge distribution of the ^{20}Ne nucleus (in its ground state) by folding the experimental charge distributions of ^{16}O and ^4He, which we already have used in our double-folding procedure, with the radial wave function $u_0(r)$ and assuming a spherical shape for the folded distribution. The result of this calculation is shown in Fig. 11 together with the experimental charge distributions, as measured by electron scattering on ^{20}Ne, and with the difference between the two curves. It can be seen that the calculation overestimates the experimental density in the nuclear interior, whereas in the surface region, near $r = 3$ fm, the experimental values are slightly underestimated. But the rms radii of both distributions come out to be identical: $\langle r^2 \rangle^{1/2} = 2.992$ fm.

VI. VOLUME INTEGRALS AND EXCITATION FUNCTIONS

The values for the volume integrals J_I of the imaginary part of the α + ^{16}O optical potential (see Table

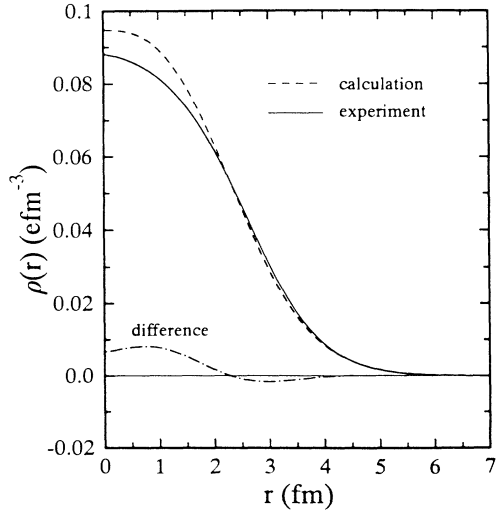

FIG. 11. Comparison of the experimental charge distribution of ^{20}Ne [58] with the distribution calculated in the potential model.

I) are shown in the upper part of Fig. 12. The energy dependence of these data can be parametrized [63] by

$$J_I = \begin{cases} J_0 \frac{(E-E_0)^2}{(E-E_0)^2+\Delta^2}, & E \geq E_0, \\ 0, & E < E_0, \end{cases} \quad (21)$$

with E_0 being the threshold energy for inelastic α scattering: $E_0 = 6.05$ MeV. A linear regression procedure to the data points results in $J_0 = 114.4$ MeV fm^3 and $\Delta = 25.8$ MeV. The curve calculated with these parameters is given in the upper part of Fig. 12 as a solid line.

For the calculation of the dispersion relation [Eq. (14)], assumptions about the energy behavior of J_I at higher energies are necessary. As already shown by Mahaux *et al.* [26] and more recently by Abele [48], the high energy behavior of J_I mainly affects the overall normalization of J_R. This uncertainty in the overall normalization is avoided by the use of the subtracted dispersion relation [Eq. (15)]. The influence of the high energy behavior of $J_I(E)$ to the real part $\Delta J_R(E)$ for energies lower than 150 MeV has been studied for three different dependencies of $J_I(E)$ [48]: (i) a linear decrease is assumed in the range 250 MeV $< E < E_L$ with $J_I(E_L) = 0$ and $E_L = 10^{20}$ MeV; (ii) an energy-independent behavior is assumed in the range 250 MeV $< E < 10^3$ MeV whereas for higher energies up to 10^{20} MeV again a linear decrease is supposed; and (iii) a linear increase in the range 250 MeV $< E < 10^3$ MeV is assumed with $J_I(10^3 \text{ MeV}) = 2J_I(250 \text{ MeV})$ together with a linear decrease at higher energies up to 10^{20} MeV. The application of the subtracted dispersion relation results in a very similar energy dependence of $\Delta J_R(E)$ in the energy range -10 MeV $< E < 150$ MeV for all three cases studied. Only differences of the order of 3% are observed. In a further study the upper energy limit E_L has been varied in the range $10^{10} < E_L < 10^{200}$ MeV. The influence of this variation to the real part $\Delta J_R(E)$ for energies lower than 150 MeV is negligible [48].

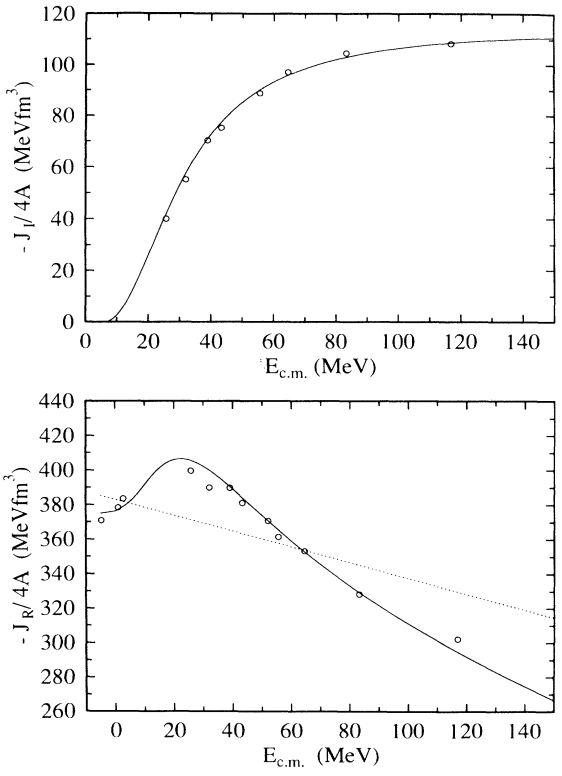

FIG. 12. Volume integrals of the real and imaginary part of the optical potential for the α + ^{16}O system: Results of the fit procedure (Tables I and IV: open circles). The solid curve for the imaginary part is given by Eq. (21) with $J_0 = 114.4$ MeVfm^3, $E_0 = 6.05$ MeV, and $\Delta = 25.8$ MeV. For the real part the volume integral of the bare channel potential is given as a dotted line, whereas the total values (channel plus dispersive part) are marked as a solid line. The normalization is done at $E_\alpha^{\text{lab}} = 80.7$ MeV.

In the calculations presented here we used the parametrization (21) up to an energy of $E = 220$ MeV whereas for higher energies up to $E_L = 10^{20}$ MeV a linear decrease of $J_I(E)$ was assumed with $J_I(E_L) = 0$. For the numerical calculation of the integral, the function J_I [Eq. (21)] was approximated by straight lines in energy intervals whose lengths $\Delta E = E_j - E_i$ are defined by $|J(E_j) - J(E_i)| = 1$ MeV fm^3. The calculations were related to a reference energy $E_s = 80.7$ MeV (lab).

In the lower part of Fig. 12 the energy dependence of the volume integral of the channel potential, derived from the double-folding procedure and normalized to the value at E_s, is shown as a dashed line. The sum of this channel potential and the calculated dispersive part is given as a solid line. This sum is independent of the reference energy E_s as long as the value of E_s is assumed to belong to the interval 50 MeV $< E_s < 100$ MeV. The figure shows distinctly the influence of the coupling of the inelastic channels, correlated with the imaginary part of the potential, to the elastic one.

These results are very close to those obtained by Mahaux *et al.* [26]. Furthermore, in the figure the volume integrals J_R, listed in Table I, are shown together with those of the potentials which describe the ^{20}Ne $= \alpha \otimes {}^{16}$O ground state and the 1^- and 3^- resonance-state energies of the $K^\pi = 0^-$ band. The energy dependence of the values obtained from the fits to the experimental data is reproduced excellently by the results of the calculations.

It should be mentioned that these results cannot simply be compared with those of Wada and Horiuchi [21]. These authors concluded that about 30% of the observed energy dependence is due to the nonlocality of the internucleus potential or equivalently due to the internucleus antisymmetrisation effect, whereas the remaining 70% are due to other origins including dynamical polarization processes. For the results presented here it appears doubtful whether it is feasible at all to disentangle the effects due to antisymmetrization and due to dynamical polarization in our approach. On the one hand, the observed energy dependence originates from the exchange contribution in the folding potential [Eq. (5)]; on the other hand it is due to the dynamical polarization processes which are taken into account in our calculations by the use of the subtracted dispersion relation [Eq. (15)]. For a more precise statement to this topic further theo-

retical work on the relation between local and nonlocal optical potentials has to be done.

Encouraged by the good agreement of the calculated volume integrals with the fits to the experimental data (Fig. 12), we extended the calculations to the resonance region, that is to the energy range $10 \leq E_\alpha \leq 30$ MeV. The shape of the real as well as the imaginary part is fixed by the folding procedure. The radius parameter κ_I (see Sec. III) was extrapolated to lower energies; the normalization factors λ_R and λ_I are fixed by the energy dependence of the volume integrals J_R and J_I, respectively, as shown in Fig. 12.

Using these interpolated potentials we calculate the excitation functions of the $\alpha + {}^{16}\mathrm{O}$ elastic scattering [4, 11] at six angles. The results are given in Fig. 13. We find good agreement between the experimental data and the results of the calculations. Only for $\Theta_{\mathrm{c.m.}} = 137.9°$ and 163.8° the calculation overestimates the experimental data at lower energies by about a factor of 2. It should be mentioned that these calculations are not adjusted to any experimental data in this energy region. The calculations were performed straightforwardly using the energy-dependent potentials obtained by the application of the subtracted dispersion relation for the real part and the parametrization (21) for the imaginary part of the potential.

Some structures of the excitation functions are predicted by the potential. They can be associated with high spin states of the rotational bands discussed in Sec. V. In Fig. 14 the phase shifts of the partial waves with

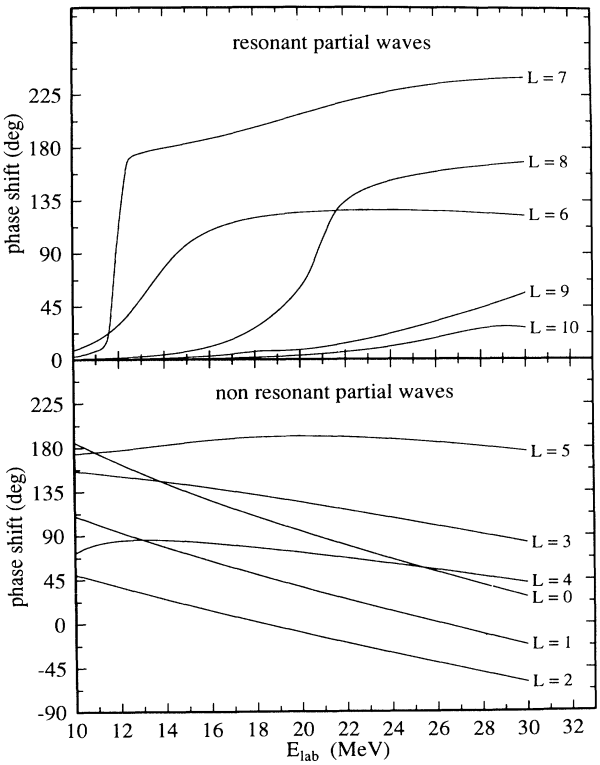

FIG. 14. Phase shifts δ_L with $L = 0$ to 10 calculated with the interpolated optical potential.

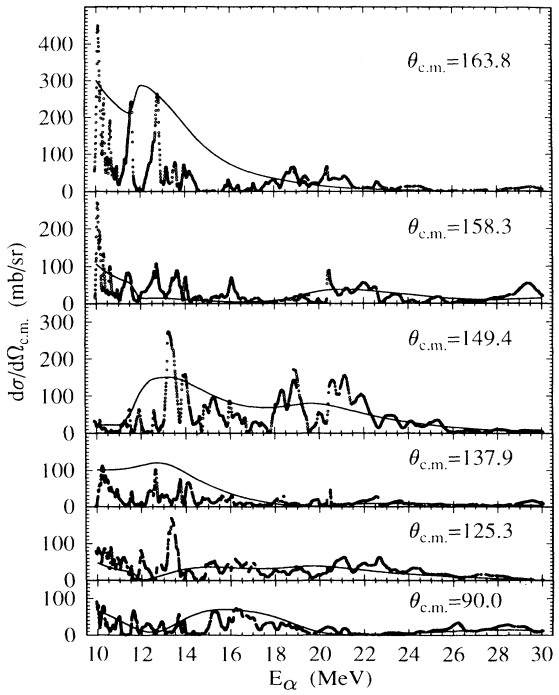

FIG. 13. Elastic α scattering on ${}^{16}\mathrm{O}$: Experimental excitation curves [4, 11] together with the results of our OM calculation.

$L = 0$ to 10 in the resonance region are shown as calculated by means of the interpolated potential. A sharp $L = 7$ resonance is found at $E_{\mathrm{lab}} \sim 11.8$ MeV; for $L = 6$ and $L = 8$ broader resonances are observed at energies near 14.5 MeV and 20.8 MeV, respectively. For $L = 9$ and $L = 10$ only weak local maxima at $E_{\mathrm{lab}} \sim 18.2$ MeV and $E_{\mathrm{lab}} \sim 29.1$ MeV are found. Due to the number of nodes of the corresponding wave functions, the $L = 7$ and $L = 9$ resonance can be associated with the 7^- and 9^- states of the $K^\pi = 0^-$ band. The resonance energies predicted by the potential model, however, are found to lie in between the experimental values given in Refs. [60] and [61], repectively (see Table IV). The $L = 6$ and $L = 8$ resonances as well as the local $L = 10$ maximum can be associated with the last three members of the $K^\pi = 0_4^+$ band in ${}^{20}\mathrm{Ne}$. This interpretation is in agreement with the results of Refs. [11, 15, 30].

VII. CONCLUSIONS

Differential cross sections for the elastic scattering of α particles on ${}^{16}\mathrm{O}$ and ${}^{15}\mathrm{N}$ have been analyzed in a wide range of energies in the framework of the optical model. The real part of the potential was deduced by a double-folding procedure using a density-dependent effective nucleon-nucleon interaction. For the imaginary part a shape of the potential similar to that of the real part was chosen. Three energy-dependent free parameters are needed to fix both parts of the potential. The

cross sections are described very satisfactorily for incident energies between about 30 and 150 MeV.

Calculations have been carried out using either zero-range or finite-range exchange terms and two different types of density dependence in the NN interaction. As a result we conclude that it is sufficient to use the numerically most convenient form of the double-folding integral which is characterized by a zero-range exchange term [42] and a density-dependence term given by Kobos *et al.* [17].

For incident energies near the Coulomb barrier we have reanalyzed the elastic $\alpha + {}^{16}$O cross section data measured by Buser [9] and McDermott *et al.* [2]. In order to fit the experimental data in this energy range using a local potential, weakly L-dependent potentials are needed. Especially the potential for the $L = 0$ partial waves results to be somewhat shallower than the potential for the other partial waves. From the optical model fits to the experimental differential cross sections phase shifts $\delta_{L=0}$ and $\delta_{L=2}$ are obtained which agree well with the results of McDermott's phase-shift analysis.

Using the double-folded α-nucleus potential as a cluster-core potential we calculate bound and quasibound states in ^{19}F and ^{20}Ne which are characterized by a moleculelike $\alpha \otimes$ core cluster structure. The excitation energies of the $Q = 8$ and 9 rotational bands in ^{19}F and ^{20}Ne as well as excitation curves in the range of the 1^- and 3^- potential resonances, electromagnetic transition rates between some states in ^{20}Ne, and the charge distribution of the ^{20}Ne nucleus are well reproduced in this potential model. Thus it may be concluded that the use of double-folded α-nucleus potentials allows a unique description of scattering cross sections as well as of bound and α-like resonance states for the systems $\alpha + {}^{16}$O and $\alpha + {}^{15}$N.

The energy dependence of the volume integral of the real potential can be understood by the combination of the slightly energy-dependent channel potential, derived from double-folding, and the strongly energy-dependent dispersive part. Using the subtracted dispersion relation [26], the observed energy dependence of the real potential can be reproduced satisfactorily.

ACKNOWLEDGMENTS

We would like to thank Prof. H. Müther and Dr. F. Hoyler for helpful discussions. The work has been funded by the German Federal Minister for Research and Technology (BMFT) under Contract No. 06 Tü 243.

[1] J.R. Cameron, Phys. Rev. **90**, 839 (1953).
[2] L.C. McDermott, K.W. Jones, H. Smotrich, and R.E. Benenson, Phys. Rev. **118**, 175 (1960).
[3] H. Smotrich, K.W. Jones, L.C. McDermott, and R.E. Benenson, Phys. Rev. **122**, 232 (1961).
[4] W.E. Hunt, M.K. Mehta, and R.H. Davis, Phys. Rev. **160**, 782 (1967); **160**, 791 (1967).
[5] J. John, J.P. Aldridge, and R.H. Davis, Phys. Rev. **181**, 1455 (1969).
[6] O. Häusser, A.J. Ferguson, A.B. McDonald, I.M. Szöghy, T.K. Alexander, and D.L. Disdier, Nucl. Phys. **A179**, 465 (1972).
[7] J.H. Billen, Phys. Rev. C **20**, 1648 (1979).
[8] J.D. MacArthur, H.O. Evans, J.R. Leslie, and H.-B. Mak, Phys. Rev. C **22**, 356 (1980).
[9] M.W. Buser, Ph.D. thesis, University of Basel (1980); Helv. Phys. Acta **54**, 439 (1981)
[10] A.A. Cowley and G. Heymann, Nucl. Phys. **A146**, 465 (1970).
[11] C. Bergman and R.K. Hobbie, Phys. Rev. C **3**, 1729 (1971).
[12] H. Oeschler, H. Fuchs, and H. Schröter, Nucl. Phys. **A202**, 513 (1973).
[13] R. Ceuleneer and F. Michel, Phys. Lett. **43B**, 365 (1973).
[14] D.A. Goldberg and S.M. Smith, Phys. Rev. Lett. **29**, 500 (1972).
[15] F. Michel, J. Albinski, P. Belery, Th. Delbar, Gh. Grégoire, B. Tasiaux, and G. Reidemeister, Phys. Rev. C **28**, 1904 (1983).
[16] H. Abele, H.J. Hauser, A. Körber, W. Leitner, R. Neu, H. Plappert, T. Rohwer, G. Staudt, M. Strasser, S. Welte, M. Walz, P.D. Eversheim, and F. Hinterberger, Z. Phys. A **326**, 373 (1987).
[17] A.M. Kobos, B.A. Brown, R. Lindsay, and G.R. Satchler, Nucl. Phys. **A425**, 205 (1984).
[18] W. Sünkel and K. Wildermuth, Phys. Lett. **41B**, 439 (1972).
[19] S. Ohkubo, Y. Kondo, and S. Nagata, Prog. Theor. Phys. **57**, 82 (1977)
[20] H. Leeb and E.W. Schmid, Z. Phys. A **298**, 113 (1980).
[21] T. Wada and H. Horiuchi, Phys. Rev. Lett. **58**, 2190 (1987).
[22] S. Yamaguchi, Phys. Rev. C **44**, 1171 (1991).
[23] T. Fliessbach, Nucl. Phys. **A315**, 109 (1979).
[24] T. Wada and H. Horiuchi, in *Proceedings of the Fifth International Conference on Clustering Aspects in Nuclear and Subnuclear Systems*, Kyoto, Japan, 1988, edited by Y. Sakuragi, T. Wada, and Y. Fujiwara, contributed papers (Physical Society of Japan, Tokyo, 1989), p. (iii)-36.
[25] E.W. Schmid, S. Saito, and M. Fiedeldey, Z. Phys. A **306**, 37 (1982).
[26] C. Mahaux, H. Ngo, and G.R. Satchler, Nucl. Phys. **A449**, 354 (1986); **A456**, 134 (1986).
[27] F. Michel, Y. Kondo, and G. Reidemeister, Phys. Lett. B **220**, 479 (1989).
[28] H. Horiuchi and K. Ikeda, Prog. Theor. Phys. **40**, 277 (1968).
[29] Y. Fujiwara, H. Horiuchi, K. Ikeda, M. Kamimura, K. Kato, Y. Suzuki, and E. Uegaki, Suppl. Prog. Theor. Phys. **68**, 29 (1980).
[30] F. Michel, G. Reidemeister, and S. Ohkubo, Phys. Rev. C **35**, 1961 (1987).
[31] R. Middleton, in *Nuclear Reactions Induced by Heavy Ions*, edited by R. Bock and W.R. Hering (North-Holland, Amsterdam, 1969), p. 263.
[32] A.A. Pilt, D.J. Millener, H. Bradlow, O. Dietzsch, P.S. Fisher, W.J. Naude, W.D.M. Rae, and D. Sinclair, Nucl. Phys. **A273**, 189 (1976).
[33] H.S. Bradlow, W.D.M. Rae, P.S. Fisher, N.S. Godwin, G. Proudfoot, and S. Sinclair, Nucl. Phys. **A314**, 207

(1979).
[34] H. Furutani, H. Kanada, T. Kaneko, S. Nagata, H. Nishioka, S. Okabe, S. Saito, T. Sakuda, and M. Seya, Suppl. Theor. Phys. **68**, 193 (1980).
[35] P. Descouvement and D. Baye, Nucl. Phys. **A463**, 629 (1987).
[36] B. Buck, C.B. Dover, and J.P. Vary, Phys. Rev. C **11**, 1803 (1975).
[37] B. Buck and A.A. Pilt, Nucl. Phys. **A280**, 133 (1977).
[38] H. Feshbach, Ann. Phys. **5**, 357 (1958); **19**, 287 (1962).
[39] G.F. Bertsch, J.Borysowicz, H. McManus, and W.G. Love, Nucl. Phys. **A284**, 399 (1977).
[40] N. Anantaraman, H. Toki, and G.F. Bertsch, Nucl. Phys. **A398**, 269 (1983).
[41] A.K. Chaudhuri and B. Sinha, Nucl. Phys. **A455**, 169 (1986).
[42] G.R. Satchler and W.G. Love, Phys. Rep. **55**, 183 (1979)
[43] J.P. Jeukenne, A. Lejeune, and C. Mahaux, Phys. Rev. C **16**, 80 (1977); J.P. Jeukenne and C. Mahaux, Z. Phys. A **302**, 233 (1981).
[44] M. Ermer, H. Clement, G. Frank, P. Grabmayr, N. Heberle, and G.J. Wagner, Phys. Lett. B **224**, 40 (1989).
[45] R. Campi and A. Bouyssy, Phys. Lett. **73B**, 263 (1978).
[46] D.T. Khoa, Nucl. Phys. **A484**, 376 (1988).
[47] D.T. Khoa, A. Faessler, and N. Ohtsuka, J. Phys. G **16**, 1253 (1990).
[48] H. Abele, Ph.D. thesis, University of Tübingen (1992).
[49] J.C. Pacheco, J.L. Ferrero, N. Vinh Mau, and B. Bilwes, Phys. Lett. B **267**, 455 (1991).
[50] F. Hinterberger, private communication.
[51] B.G. Harvey, E.J.-M. Rivet, A. Springer, J.R. Meriwether, W.B. Jones, J.H. Elliot, and P. Darriulat, Nucl. Phys. **52**, 465 (1964).
[52] M. Reed, Ph.D. thesis, University of California (1978).
[53] G. Hauser, R. Löhken, H. Rebel, G. Schatz, G.W. Schweimer, and J. Specht, Nucl. Phys. **A128**, 81 (1969).
[54] K.T. Knöpfle, G.J. Wagner, H. Breuer, M. Rogge, and C. Mayer-Börike, Phys. Rev. Lett. **35**, 779 (1975).
[55] B.G. Harvey, J.R. Meriwether, J. Mahoney, A. Bussiere de Nercy, and D.J. Horen, Phys. Rev. **146**, 712 (1966).
[56] H. Abele, H. Jäntsch, R. Neu, G. Staudt, C. Striebel, P.D. Eversheim, F. Hinterberger, and H.J. Gils, Verhandl. DPG(VI) **23**, 217 (1988)
[57] P. Grabmayr, private communication.
[58] H. de Vries, C.W. de Jager, and C. de Vries, At. Data Nucl. Data Tables **36**, 495 (1987).
[59] H. Abele, computer code GOMPF, University of Tübingen (unpublished).
[60] F. Ajzenberg-Selove, Nucl. Phys. **A475**, 1 (1987).
[61] F. Ajzenberg-Selove, Nucl. Phys. **A392**, 1 (1983).
[62] P.N. Endt, At. Data Nucl. Data Tables **23**, 3 (1979).
[63] C. Mahaux, P.F. Bortignon, R.A. Broglia, and C.H. Dasso, Phys. Rep. **120**, 1 (1985).